Electronic Structure of Adenine and Thymine Base Pairs Studied by Femtosecond Electron−Ion Coincidence Spectroscopy

Niklas Gador,[†] Elena Samoylova,[‡] Valoris Reid Smith,[‡] Albert Stolow,[†] David M. Rayner,[†] Wolfgang Radloff,[‡] Ingolf Volker Hertel,[‡] and Thomas Schultz*[,‡]

Steacie Institute for Molecular Sciences, National Research Council, 100 Sussex Drive, Ottawa, K1A 0R6 Canada, and Max Born Institute, 12489 Berlin-Adlershof, Germany

Received: August 24, 2007; In Final Form: September 6, 2007

Femtosecond pump−probe spectroscopy was combined with photoelectron−photoion coincidence detection to investigate the electronic structure and dynamics of isolated adenine (A) and thymine (T) dimers and the adenine−thymine (AT) base pair. The photoelectron spectra show that $\pi\pi^*$ and $n\pi^*$ states are only weakly perturbed in the hydrogen-bound dimers as compared to the monomers. For cationic base pairs with internal energies greater than 1 eV, we observed considerable cluster fragmentation into protonated monomers. This process selectively removed signals from the $n\pi^* \rightarrow n^{-1}$ ionization channel in all dimers. The photoelectron spectra are compared to time-resolved mass spectra and confirm the assignment of short-lived $\pi\pi^*$ and $n\pi^*$ populations in the adenine, thymine, and mixed AT dimers.

I. Introduction

Biological materials on earth are constantly exposed to potentially harmful UV radiation from the sun. In order to remain viable, biological systems must therefore have ways of dealing with this danger. Research into the UV photophysics of DNA is receiving increasing interest because it is assumed that DNA must have some inherent photoprotection mechanisms.[1,2] Studies targeting small, isolated DNA constituents[3−11] complement work on DNA multimers in the liquid phase[12] in terms of understanding the complex photophysics of DNA in its natural biological environment. Small molecular clusters in the gas phase can mimic important structural elements of DNA and thus help to extend the power of gas-phase spectroscopic methods to increasingly complex systems.[13−18] Here we report a direct characterization of the electronic structure for photoexcited states in DNA base pairs of adenine and thymine and correlate the structure with corresponding dynamic processes using femtosecond time-resolved electron−ion coincidence (FEICO) spectroscopy.[19,20]

The photophysics of the isolated adenine monomer has been investigated in some detail. Photochemical excitation of the S_2 ($\pi\pi^*$) state is followed by rapid internal conversion on a picosecond to femtosecond time scale.[3,5,8−11,15,16] Internal conversion can populate the S_1 ($n\pi^*$) state, as proposed by theory[21] and spectroscopic and dynamic measurements.[3,6,22] The strong mixing of $\pi\pi^*$ and $n\pi^*$ states was confirmed by time-resolved photoelectron spectroscopy[8,9] and by rotational band contour analysis.[23] Internal conversion time scales were reported to be 40−100 fs at excitation energies of ≤267 nm.[8−11,15] In this wavelength range, the $n\pi^*$ state decays with a lifetime of ∼1.2 ps to the ground state and several internal conversion pathways were proposed to explain this fast radiationless transition. Out-of-plane deformation of the six-membered ring can lead to conical intersections between $n\pi^*$, $\pi\pi^*$, and the ground state with very small barriers.[21,24−26] A conical intersection to a quasi-dissociative $\pi\sigma^*$ may also play a role,[8,11] especially at higher excitation energies or in polarizable environments.[16,27−30]

Time-resolved photoelectron spectroscopy (TRPES) experiments comparing adenine with 9-methyl-substituted adenine[11] found the same biexponential time constants, 0.1 and 1.2 ps, as ion yield studies.[10,18] But different decay-associated photoelectron spectra of the 0.1 ps component were assigned to the participation of a $\pi\sigma^*$ state based on calculations of the Franck−Condon spectra. The reduction in yield of the $n\pi^*$ signal relative to the $\pi\pi^*$ signal in adenine as compared to 9-methyl adenine[10,11] provided additional evidence of a competing ultrafast channel.

At first glance, the situation in thymine resembles that of adenine: the optically bright S_2 ($\pi\pi^*$) state can internally convert into the S_1 ($n\pi^*$) state[31,32] with subsequent radiationless transition into the ground state. Corresponding decay properties were found with a fast initial process ($\tau \leq 100$ fs) followed by a picosecond decay ($\tau = 6-10$ ps).[9,33] It was proposed that the $\pi\pi^*$ state internally converts to the $n\pi^*$ state[2,31] or a low-lying biradical state[34] within 100 fs. But an additional long-lived state is observed with a lifetime of $\tau = 22$ ns[7] and the state assignment remains subject of debate. The existence of two distinct $n\pi^*$ states or the population of triplet states may explain the complex dynamics. However, an alternate proposal is that the thymine S_2 state is long-lived relative to that in adenine and the observed sub-100 fs dynamics are due to vibrational energy redistribution (IVR). IVR may then be followed by crossing to the long-lived S_1 state on a ps time scale.[35]

For the adenine−thymine base pair, molecular dynamics/ab initio studies predicted predominantly planar, hydrogen-bound structures.[36] However, the Watson−Crick (WC) structure was not the lowest energy structure and was also not identified in nanosecond IR-UV resonance-enhanced multiphoton ionization (REMPI) experiments in a supersonic jet expansion.[37] An excited-state hydrogen transfer process may accelerate the excited-state relaxation of $\pi\pi^*$ states in the Watson−Crick

* Corresponding author. E-mail: schultz@mbi-berlin.de.
[†] Steacie Institute for Molecular Sciences.
[‡] Max Born Institute.

10.1021/jp076800e CCC: $37.00
Published on Web 10/31/2007

structure but not in the lowest energy structure.[2,38] A short excited-state lifetime hampers detection via nanosecond REMPI and offers an alternative explanation for the absence of WC structures in the corresponding experiments. In a model system, the hydrogen transfer and resulting accelerated excited-state relaxation was observed;[14,39] hence, such a process is accessible to characterization by femtosecond pump−probe experiments. Femtosecond time-resolved experiments showed similar excited-state dynamics in base monomers and dimers[15] and proposed that the same $\pi\pi^*$ and $n\pi^*$ states are involved in the excited-state relaxation of all species. In the dimers, an additional quenching of the $n\pi^*$ state was assigned to a relaxation via the $\pi\sigma^*$ state.[16]

TRPES is a powerful technique that can follow excited-state nonadiabatic processes in real time and often allows for the unambiguous assignment of excited-state character along a reaction coordinate.[40−42] Hence, TRPES should be the method of choice to identify changes in the electronic character between base monomers and dimers. The investigation of molecular clusters, however, requires the additional identification of cluster species because the emitted electrons cannot be distinguished a priori. This became feasible with the development of the FEICO coincidence technique[19,20] and was applied to a number of small molecular clusters successfully.[43] Here we apply the FEICO technique for the first direct identification of the electronic character of excited states in adenine and thymine base pairs and to identify relevant processes in the excited and ionic states. Because no isomer selection is possible in these experiments, we study the sum of signal contributions from all base pair isomers in the cluster beam. FEICO measures the energy partitioning between emitted electron and remaining ionic core; hence, cluster fragmentation processes in the ion can be directly related to the internal energy.

II. Experiment

Details of the FEICO experimental setup and DNA base cluster spectroscopy have been described elsewhere.[15,20] In brief, adenine and thymine (Sigma-Aldrich, 99% purity) were evaporated in an oven at 200−220 °C. The vapor of both compounds was entrained in helium (1 bar) and expanded through a high-temperature pulsed valve (General Valve, Series 9, modified for temperatures up to 300 °C) into the source chamber, $P_{\text{background}} \approx 10^{-5}$ mbar. The valve operated at 120 Hz and limited the repetition rate for our measurements. The expansion generated a supersonic molecular beam containing a distribution of monomers, both homo- and heterodimers and some larger clusters. A conical nozzle in front of the valve increased the number of collisions and aided clustering. The cluster size distribution was controlled by adjusting the He buffer gas pressure, the pulsed valve opening time, and the timing between the laser pulses and the valve opening. The molecular beam was skimmed as it entered the interaction chamber, $P_{\text{background}} \approx 10^{-6}$ mbar. In the interaction region, the molecular beam was crossed by the co-propagating femtosecond pump and probe laser pulses. The probe laser pulse generated both ions and electrons. Immediately after the probe pulse, a 300 ns field-free period permitted collection of the electrons, which were analyzed in a magnetic bottle time-of-flight electron spectrometer. To ensure collection of slow electrons, a weak DC electric field of ~0.1 V/cm was applied in the interaction region. After the 300 ns period, the ions were extracted with a pulsed electrical field into a Wiley−McLaren time-of-flight (TOF) mass spectrometer. Both spectrometers axes were arranged perpendicularly to the molecular beam direction and to the direction of laser light propagation.

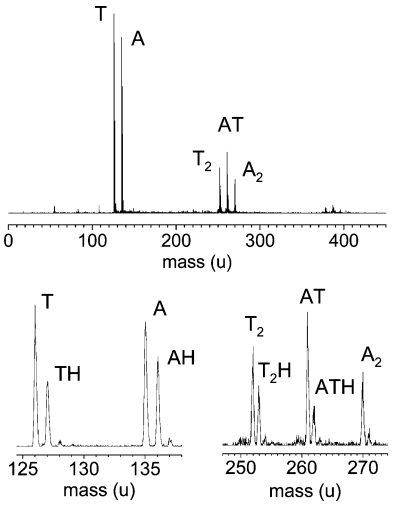

Figure 1. Mass-spectrum of adenine (A) and thymine (T) cluster cations recorded at zero delay time between pump and probe laser pulses at 266 and 400 nm. Signals in the mass channel of protonated species (XH, see enlarged insets) arise from fragmenting clusters.

The pump and probe laser beams were generated by a commercial Ti:Sapphire oscillator and amplifier system (Clark MXR, operating at 1 kHz). In all cases, the third harmonic of the laser output at 266 nm was used as the pump. The multiphoton probe pulse was either the second harmonic at 400 nm or the fundamental at 800 nm. The pump pulse fluence was $<3 \times 10^{10}$ W/cm^2 and the 400 nm probe pulse had a fluence of $<1.5 \times 10^{12}$ W/cm^2. These relatively low fluences resulted in small ionization probabilities of <10%. This is essential to avoid false coincidences[20] and unwanted multiphoton transitions of higher order. The cross correlation width (time resolution) was ~140 fs. A stepper motor-controlled delay stage adjusted the time delay between the pump and probe pulse. Electrons and ions were counted in coincidence using a Lecroy 4208 time-to-digital converter. Data for 5×10^5 to 8×10^6 laser pulses was acquired for a single coincidence spectrum. Pump-only and probe-only spectra were measured separately and subtracted from the pump−probe data.

The photoelectron kinetic energy was calibrated using one-color multiphoton ionization of NO and Xe. At small electron energies (<0.25eV), stray electric fields and imperfections of the magnetic field may effect the electron detection efficiency and distort the photoelectron spectra.

III. Results and Discussion

A. Cluster Mass Spectra and Fragmentation Channels. We begin by establishing which species are present in the molecular beam. In Figure 1, we show a cluster mass spectrum of adenine and thymine recorded at delay time zero using laser wavelengths of 266 and 400 nm for the pump and probe pulses, respectively. The formation of A_2, T_2, and the AT base pair is evident, as is the presence of a small amount of trimer clusters. With the low laser fluence used in our experiments, the dominant ionization channel is one-photon excitation at 266 nm, followed by two-photon 400 nm ionization. The overall cluster distribution was narrow to minimize signal contributions from fragmentation of trimers and higher clusters, which might distort the observed dimer signals.[15]

A striking feature in the mass spectrum is the appearance of large peaks with mass-to-charge ratios (m/z) corresponding to protonated monomers and protonated base pairs. These can only arise from fragmentation of larger cationic clusters, preceded

by a proton transfer in the cationic state or perhaps by hydrogen transfer in the neutral excited state. The mass M + 1 isotopomers (due to the natural abundance of ^{13}C and ^{2}D isotopes) also contribute to these mass peaks, but explain only a small fraction of the signals: we expect only 7% and 6% of natural M + 1 isotopes for A and T, repectively.

The detection of significant amounts of protonated base monomers and dimers implies the occurrence of proton/hydrogen transfer coupled with cluster fragmentation. In the collision-free environment of a molecular beam, the only possible source of proton or hydrogen is a partner base in the cluster. The transfer can occur prior to ionization in the neutral excited states or after ionization in the cation. Hydrogen transfer in the neutral excited state would drastically affect the pump−probe photoelectron spectrum and the excited-state dynamics as observed previously in the base pair model aminopyridine dimer.[14,39,44,45] Our data show no evidence for this process (see ref 15 and our discussion of electron spectra and dynamics below). Proton transfer and fragmentation in the ion, however, has also been suggested for the radical cation of cytosine−guanine base pairs and may have important implications for DNA damage by ionizing radiation.[4]

From the measured acidity of the A radical cation (221 kcal/mol; 9.58 eV)[46] and the proton affinity of A (225 kcal/mol; 9.76 eV),[47] the proton-transfer step in the A_2 cation is exothermic by 4 kcal/mol (0.17 eV). The acidity of the T radical cation is not available to assess this process in T_2, but the observation of protonated T in T-cluster spectra (data not shown here) indicates that the corresponding process is also energetically neutral or exothermic. In this case, the calculated and experimental proton affinity of T (209 kcal/mol; 9.06 eV)[47,48] places a limit of <209 kcal/mol on the acidity of the T radical cation. On the basis of this estimate for T cation acidity, transfer from the T cation to A is exothermic by >17 kcal/mol (0.74 eV).

The proton affinities for T are smaller than those for A, and the proton transfer from A cation to T is endothermic by ∼11 kcal/mol (0.49 eV). However, the later process must compete with electron transfer, which can move the charge from T^+ to A (exothermic by 0.70 eV based on the respective ionization potentials). A second mechanism that can lead to the protonated monomers is hydrogen atom transfer in the ionic state followed by dissociation, but insufficient thermodynamic data are available to assess such processes. To summarize, we may expect protonated A after exothermic proton transfer in A_2 and AT and protonated T after the corresponding reaction in T_2. This thermodynamic analysis is valid for the ionic ground state; the outcome may be altered at higher internal energies and/or in electronically excited states.

B. Cluster Photoelectron Spectra. FEICO spectra for the A and T monomers and dimers are shown in Figure 2. The total energy ($E_{h\nu}$) available from pump plus probe photon absorption is partitioned between the electron binding energy, the internal degrees of freedom in the cation, and the kinetic energy (E_{el}) of the emitted electron. The first two terms can be characterized by the vertical (band maximum) or adiabatic (threshold) ionization potentials (IP), calculated from measured electron energies using $E_{el} + IP = E_{h\nu}$. For our 267 nm + 2 × 400 nm ionization process, the photon energy $E_{h\nu}$ is 10.85 eV. The photoelectron spectra associated with the A and T monomer are consistent with previous measurements made for the isolated bases.[8,9] Two broad bands correspond to ionization into the D_0 (π^{-1})/D_1 (n^{-1}) cation states with vertical ionization potentials of 8.48/9.58 eV for adenine[49] and 9.18/10.03 eV for thymine.[50] According to a Koopmans' correlation analysis (see refs 41 and 42 for a detailed discussion), the bands reflect the Franck−Condon envelope for the S_2 ($\pi\pi^*$) → D_0 (π^{-1}) and S_1 ($n\pi^*$) → D_1 (n^{-1}) transitions. Our observed vertical ionization potentials for adenine and thymine (i.e., the maxima of the photoelectron bands in Figure 2) are located about 0.3 eV above the energies calculated for the vertical ionization potentials in the literature. This can be related to the excess vibrational energy of ∼0.2 and ∼0.3 eV in the excited electronic states of adenine[3] and thymine,[51] which is transferred to the ionic states according to Franck−Condon probabilities.

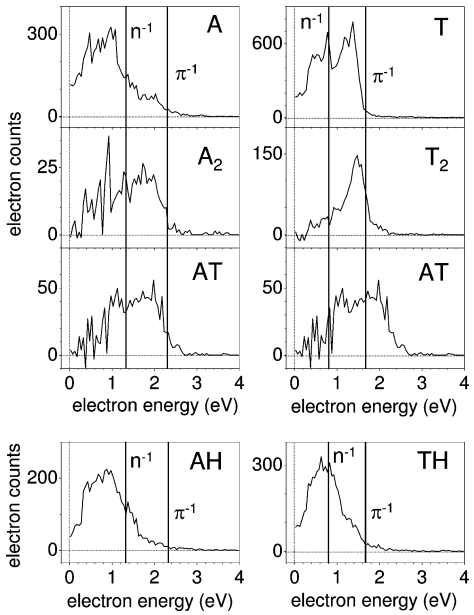

Figure 2. FEICO spectra of electrons coincident with the masses of the cationic adenine and thymine bases and base pairs (top) and the protonated base monomers (bottom) as shown in Figure 1. The vertical lines indicate literature values for the vertical ionization potentials into the D_0 (π^{-1}) and D_1 (n^{-1}) states of A and T (see text). The adenine−thymine spectrum is shown in both columns for easy comparison. The collection efficiency falls off for slow electrons with energies <0.25 eV, a region of uncertain amplitude (see experimental section). The ordinates show true amplitudes in counts/50 meV bin.

Analysis of the dimer FEICO spectra in Figure 2 must take possible fragmentation channels into account. If a cluster ion fragments before mass analysis, then the corresponding electrons will be assigned to the smaller (daughter) mass channel of the fragmentation product. Fragmentation rates depend on the excess energy in the ion and may therefore distort the corresponding photoelectron spectrum of the parent. Photoelectrons with high kinetic energies correlate with low cationic states that do not have sufficient energy to fragment, whereas electrons with low kinetic energy correspond to cations with large excess energies that may fragment rapidly. Here, only the base monomers and dimers are of interest. The effect of fragmentation must therefore be minimized by reducing the width of the cluster distribution, removing higher clusters from the molecular beam. This avoids "fill-in" effects, that is, fragmentation of larger clusters into the dimer mass channels and resulting increased signals in the FEICO spectra. We investigated different cluster distributions and found fill-in effects for the dimers with electron energies <1.2 eV when there was a broad cluster distribution. Fragmentation of dimers can also displace the signal into the monomer or protonated monomer mass channel. We observed only small changes in the photoelectron spectra of nonprotonated base monomers in the presence or absence of clusters. Hence, fill-in effects appear to be of minor importance for the unprotonated species. The protonated monomers, however, appear only as

fragmentation products and are due exclusively to cluster fragmentation.

Fragmentation also leads to "drop-out" effects in the cluster signal, that is, loss of FEICO signal due to fragmentation of the cationic base pairs. As a result, photoelectrons that should be in coincidence with the dimer cation are measured in coincidence with the protonated monomer fragments instead. Just like fill-in, drop-out effects can occur only in the low-kinetic-energy region of the FEICO spectrum corresponding to cations with sufficient internal energy for fragmentation. Drop-out explains the low intensity of <1.2 eV electrons in all dimer spectra in Figure 2. We will estimate the affected energy range in the photoelectron spectrum by unimolecular reaction theory below. Because the magnitude of the drop-out and fill-in signals must be identical, the sum of the electron signals from the unfragmented dimers and the protonated monomer fragmentation products should yield the undistorted photoelectron spectrum of the dimers.

Fragmentation does not affect the spectral region of high electron energy. The A_2 electron spectrum closely mirrors that for ionization into the $D_0(\pi^{-1})$ ionic state in the A monomer and shows a similar vertical ionization potential. For T_2, both vertical and adiabatic ionization potentials are reduced by ~0.25 eV as compared to the T monomer. The AT electron spectrum is almost identical to that of A_2. The nearly identical spectra of AT and A_2 suggests that excitation of AT at 266 nm occurs mainly in the A chromophore. This is in accord with recent calculations of excited-state character and oscillator strength in AT base pairs[2] and spectroscopic results at lower excitation energies.[37] However, the observed excited-state dynamics discussed below show that excitation and ionization of the T chromophore in AT also plays a role. On the basis of the previous discussion of reactions in the cluster radical cations, we can offer an alternative explanation for the weakness of T spectral features in the AT electron spectrum: Excitation and ionization of the T chromophore in AT can be followed by exothermic electron or proton transfer and rapid cluster dissociation, removing the corresponding signal from the AT mass channel.

Fragmentation removes the spectral region of low electron energies from the mass channels of dimers into those of the protonated monomers. Ionization into the $D_1(n^{-1})$ state of A leads to hot ions with >1.1 eV excess energy. The corresponding electron band from the A dimer is very similar to that of the monomer but is observed in the protonated fragmentation product AH. For T, the $D_1(n^{-1})$ ionic state carries >0.8 eV excess energy and again the corresponding dimer band is observed in the protonated fragmentation product TH. The similarities of the monomer and dimer electron spectra, the latter observed in dimer and protonated monomer mass channels, indicate that the electronic structure of the bases is only weakly perturbed in the hydrogen-bonded complex. This seems to be true for both, the $\pi\pi^* \rightarrow \pi^{-1}$ and $n\pi^* \rightarrow n^{-1}$ ionization processes. We therefore have the first direct spectroscopic evidence for nearly unperturbed $\pi\pi^*$ excited and π^{-1} ionic states in the base dimers.

Time-of-flight (TOF) mass spectrometry with pulsed-field ion extraction imposes a gate on the time available for cation fragmentation. If an excited ion fragments before the ion extraction field is turned on (300 ns in our case), then the TOF is that of the daughter cation. If fragmentation occurs in the acceleration zone (300 ns < Δt < 1.8 μs), then the TOF is in between that of the parent and daughter cation. Because there is a distribution of fragmentation times, such signals will be smeared out across a large region of the mass spectrum and cannot be assigned to any mass. If fragmentation occurs after the acceleration zone (Δt > 1.8 μs), then the TOF is identical to that of the nonfragmenting cation. To bracket the likely range of electron energies where the FEICO spectrum remains undistorted, we performed RRKM calculations for the case of A_2.

The binding energy for the A_2 cation separating into A + A^+ is estimated to be about 1 eV using measured ionization potentials for the neutral monomer and dimer[52] in conjunction with the calculated neutral dimer ground-state binding energy.[36] The proton transferred cation, $(AH^+)(A-H)$, is expected to have a lower binding energy as seen for guanine−cytosine by Nir et al.,[4] and we have adopted a value of 0.8 eV. Adenine vibrational frequencies were taken from DFT calculations by Lappi et al.,[53] and six additional vibrations, set to 150 cm^{-1}, were added to account for the extra degrees of freedom in the dimer. The calculation is relatively insensitive to this parameter. We treated the Arrhenius A-factor as a variable and adjusted it by softening these six frequencies in the transition complex. We find that for an A-factor of 10^{14}, the internal energy of the cation must be less than 1.4 eV for it to be detected as an intact complex. This value rises to 1.65 eV if the A-factor is 10^{13} and drops to 1.25 eV if it is 10^{15}. The electron energy, E_{el}, is related to the cation internal energy, E_{int} by

$$E_{el} = E_{h\nu} + E_{th} - IP_a - E_{int}$$

where $E_{h\nu}$ is the total photon energy, E_{th} is the initial thermal energy in the neutral dimer, and IP_a is the adiabatic ionization potential. The initial thermal excitation is negligible for the supersonic beam conditions employed here. With $E_{h\nu} = 10.85$ eV and $IP_a \approx 8.2$ eV (see ref 54 and references therein), this means that only photoelectrons with E_{el} > 1.2 eV will be detected in coincidence with their parent ion; that is, only for kinetic energies above this value will the coincident photoelectron spectrum be undistorted by fragmentation. This agrees well with the observed spectra in Figure 2: the A_2 signal drops for electron energies <1.2 eV and the signal of the AH^+ fragmentation product is rising correspondingly. Note that although fragmentation distorts the low-energy portion of the spectrum a significant portion of the spectrum at high energies is unaffected. From the analysis of the corresponding region in our photoelectron spectra, we obtain vertical ionization potentials of ~ 9 eV for A_2 and AT, similar to that of the A monomer in the same excitation−ionization process. The values are higher than literature values of 8.48 eV for the ground-state ionization of adenine[49] because of vibrational excitation in the pump (excitation) step and correspondingly different Franck−Condon factors in the probe (ionization) step. For T_2, we found an IP_V of 9.35 eV, about 0.25 eV lower than the respective value for the T monomer in the same ionization process (compare to the ground-state ionization potential of 9.18 eV for T[50]).

C. Ultrafast Decay Dynamics. The excited-state dynamics for base pairs of adenine and thymine were presented in the description of earlier femtosecond pump−probe experiments using ion detection.[15] In Figure 3, we present new time-dependent ion signals including the data for the protonated monomers. The cationic fragmentation products AH and TH are shown in the presence and absence of the mixed AT cluster to distinguish dynamic processes prevalent in A and T clusters from those in the mixed cluster. The displayed range of delay times is restricted to 5 ps because photoelectron spectra have been measured only in this time window. Preliminary experiments on longer pump−probe time scales show several con-

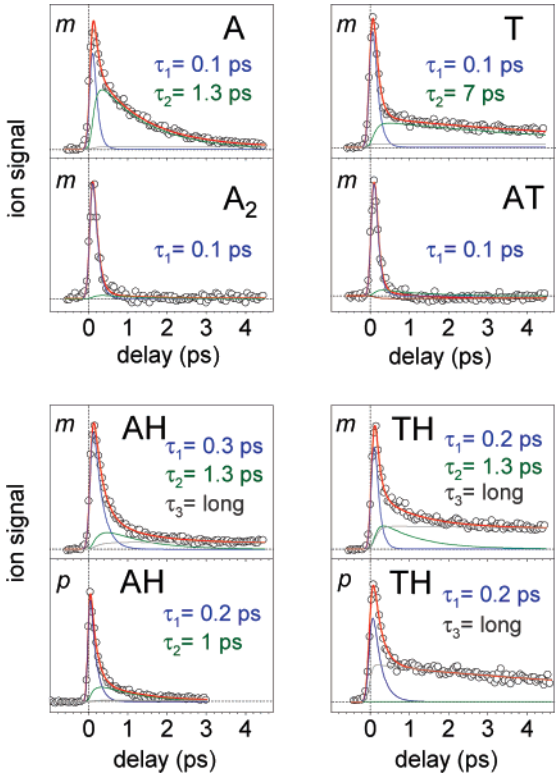

Figure 3. Integrated ions signals of bases, base pairs, and protonated bases as a function of the delay time between the 266 nm pump and 800 nm probe pulses. The protonated bases in the presence of the mixed AT base pair (*m*, top traces) show more complex dynamics than the corresponding signals for pure A or T clusters in absence of mixed clusters (*p*, bottom traces). The fit curves (thick lines) are the sum of several monoexponential decay components (thin lines) convoluted with the Gaussian laser cross-correlation function. Lifetimes τ_n are indicated for the dominant decay components. The τ_3 component is assigned to the T chromophore (see text).

tributions to the long lifetime τ_3 due to clusters containing T. The origin of this decay process will be elucidated in a forthcoming, more-detailed study. The dynamics of A and T monomers are characterized by two time constants τ_1 and τ_2, which are in agreement with earlier results.[8,15] An additional state with a nanosecond lifetime exists in T[7] but plays no role in our discussion.

The lifetimes τ_1 characterize the decay of the photoexcited $\pi\pi^*$ states, whereas lifetimes τ_2 reflect the relaxation of the subsequently populated $n\pi^*$ states. The ion signals of A_2, T_2 (not shown), and AT show only the ultrafast decay of the initially excited $\pi\pi^*$ state with the time constant τ_1. Because of fragmentation, the signal contributions with time constant τ_2 are very weak in the dimer mass channels but appear instead for the protonated fragmentation products AH and TH. This reflects the higher energy of the ionic states accessed by $n\pi^* \rightarrow n^{-1}$ ionization and the resulting proton transfer and fragmentation reactions discussed above. The fragmentation efficiency following $\pi\pi^* \rightarrow \pi^{-1}$ ionization is significantly lower but non-negligible and the corresponding τ_1 transient is present in both dimer and protonated monomer mass channels, albeit with slightly different lifetimes. Those differences may reflect the evolution of the excited-state geometry and corresponding changes in the Frank−Condon factors for ionization from the $\pi\pi^*$ state into lower/higher vibrational states in the ion. Similar lifetime differences as a function of fragmentation channel were observed in pump−probe fragmentation via the $\pi\pi^*$ state of protonated adenine.[55]

An alternate explanation for protonated ion signals could be hydrogen transfer in the neutral excited state followed by ionization and fragmentation. In this case, we would expect a delayed rise of the protonated monomer signals, reflecting the rate of the H-transfer process in the excited state. This stands in contrast to the immediate rise at delay time zero of the protonated monomer signals in Figure 3. Furthermore, the subsequent excited-state relaxation dynamics should be strongly affected and would no longer resemble those observed for the base monomers. On the time scale of our experiment, we observed neither a delayed rise nor any specific decay dynamics in the protonated monomers and therefore suggest that, at 267 nm excitation, H transfer in the neutral is a minor channel.

We now consider the protonated monomer signals AH and TH in a mixed cluster beam (trace *m* in Figure 3) containing A, T, and AT clusters. Assuming mainly intramolecular relaxation in the base pairs and therefore relaxation rates similar to the monomers (compare to ref 15), the time constant $\tau_2 \approx 1$ ps reflects the $n\pi^*$ decay in A, and the long time constant τ_3 contains the corresponding 7 ps and slower decays in T. The τ_2 and τ_3 decays are observed in both the AH and TH fragments, albeit with different amplitudes. The different weights of the weak contribution with 7 ps decay time to the TH signal for mixed and pure clusters explain the slightly different decay behavior of the long decay component τ_3. The long decay component τ_3 is absent in the AH signal of pure adenine clusters (trace *p* in Figure 3) and must stem from the fragmentation of mixed AT clusters. We therefore assign the τ_3 decay in AH to the excitation and ionization of the thymine chromophore in AT, followed by proton transfer and fragmentation in the ion. Conversely, the decay with $\tau_2 = 1.3$ ps is absent in the TH signal of pure thymine clusters (trace *p* in Figure 3) and must also stem from the fragmentation of AT, presumably upon excitation and ionization of the A chromophore. Thus, we have evidence that both A and T chromophores can be excited and ionized in the AT dimer. Furthermore, the excited-state lifetimes in AT resemble those in the corresponding homodimers of A and T. Note that the thermodynamic analysis presented earlier predicted only the protonation of A by the T cation as an exothermic reaction channel in the ionic ground state, but we observe the protonation of T by the A cation as well.

If the dimer photophysics are dominated by intramolecular relaxation of the A or T chromophores, then the sum of protonated monomer and the dimer traces (i.e., the true dimer traces before fragmentation) should reproduce the dynamics in the monomer traces. This statement is qualitatively correct for T. For A, in contrast, the A_2 and AH signals from pure A clusters reveal a suppressed τ_2 component as compared to the monomer. This indicates that the excited-state population in A_2 may be quenched by an additional ultrafast relaxation pathway. Possibly, the stabilization of the $\pi\sigma^*$ state in the dimer leads to a coupling with the $\pi\pi^*$ state at the expense of the $n\pi^*$ state.[16]

The results of FEICO spectroscopy at pump−probe delays of 0 and 500 fs for the adenine monomer and dimer are shown in Figure 4. As in the time-resolved ion traces (Figure 3), we used a three photon 800 nm ionization process in these experiments. This ionization process allows us to partially discriminate the dynamics of the $\pi\pi^*$ state of excited A_2: For the 266 nm + 3 × 800 nm excitation-ionization process ($E_{h\nu} = 9.3$ eV), the only ionization channel leads to the D_0 (π^{-1}) state of the cation. Detection of the $n\pi^*$ state by ionization to the D_1 (n^{-1}) state requires absorption of an additional 800 nm photon, and the signals for this higher order process are weak.

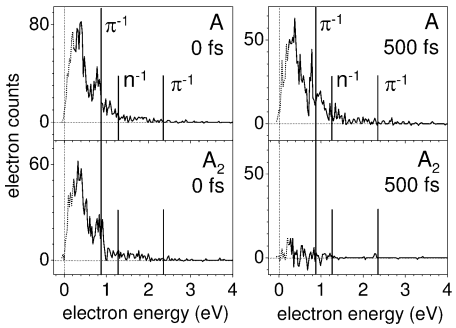

Figure 4. FEICO spectra of the adenine monomer and the adenine dimer, recorded at zero and 500 fs delay time between the 266 nm pump and 800 nm probe pulses. The long vertical lines indicate the electron energy corresponding to the adenine vertical ionization potential into D_0 (π^{-1}) by a three photon probe process. The short vertical lines indicate the corresponding electron energies associated with ionization into the D_0 (π^{-1}) and D_1 (n^{-1}) states by a four photon probe process.

Comparing the photoelectron spectra of the adenine monomer at $t = 0$ and $t = 500$ fs (Figure 4), we observe a significant signal reduction in the low-electron-energy range, reflecting the ultrafast decay of the initially excited $\pi\pi^*$ state, which was ionized by three probe photons of 800 nm. Because the lifetime of this state is $\tau_1 < 100$ fs (see Figure 3), this component should completely vanish at $t = 500$ fs. Therefore, the remaining signal at 500 fs must be attributed to the $n\pi^*$ state detected by the four photon probe. This means, however, that the zero delay time spectrum of adenine may already contain a significant signal from the $n\pi^*$ state in addition to the initially populated $\pi\pi^*$ state. The integrated electron spectrum of the adenine monomer drops in intensity to about 75% over the first 500 fs, which is in good agreement with the corresponding time-resolved trace in Figure 3.

The situation is different in the case of the dimer for which no signal of the $n\pi^*$ state is observed. Besides a possible signal reduction due to an additional relaxation channel (maybe via the $\pi\sigma^*$ state, see above), the ion fragmentation leads to a complete suppression of this signal. In the absence of signal from the $n\pi^*$ state, we can attribute the zero time delay spectrum to the $\pi\pi^*$ state. After 500 fs, this signal decays to the baseline. This confirms complete $\pi\pi^*$ state relaxation with the measured lifetime τ_1 in the A ion signals.

IV. Conclusion

The FEICO method extends the power of TRPES to molecular clusters and allows the assignment of electronic states in a local cluster environment. Here we used FEICO to identify the $\pi\pi^*$ and $n\pi^*$ character of excited states in adenine and thymine base pairs, which was previously inferred only indirectly. The clear assignment allowed us to disentangle the corresponding excited-state decay dynamics and showed that both chromophores can be excited and ionized in the cluster. On the femtosecond to few-picosecond time scale, the characteristic decay times and spectral signatures of the dimer states (and fragmentation products) are very similar to the corresponding ion yield dynamics[15] as well as the TRPES spectra[9,11] of the monomers. We interpret this as further evidence for a predominantly intramolecular excited-state character in the dimers. This also holds for the AT base pair as formed in the molecular beam: the corresponding electron spectra showed no additional bands that might be assigned to an excited-state electron−proton transfer state predicted for the Watson−Crick isomer.[2] This may be due to a non-Watson−Crick cluster structure of AT in the molecular beam[36,37] and highlights the need for a combination of structure-selective and time-resolved techniques in this field.

Fragmentation of ionic clusters is a major complication in the analysis of cluster spectra. We used FEICO to characterize the energy partitioning between emitted photoelectrons and the ionic core to obtain energetic information about fragmentation channels. Together with RRKM calculations, this offered a convincing model for the relevant fragmentation processes in the base dimer cations. The near-complete fragmentation of energetic D_1 (n^{-1}) ions into protonated base monomers helped to explain the weak $n\pi^* \rightarrow n^{-1}$ spectral and dynamic features in photoelectron and time-resolved mass spectra. Fragmentation also explained the absence of T spectral features in the AT mass channel, which can undergo exothermic electron (and subsequent proton) transfer followed by fragmentation of the cluster.

Acknowledgment. We thank Dr. F. Noack for his support by providing the laser system in the femtosecond application laboratory of the Max-Born-Institut Berlin. Financial support by the Deutsche Forschungsgemeinschaft through SFB-450 is gratefully acknowledged. N.G. thanks NSERC for funding. We thank H.-H. Ritze and H. Satzger for helpful discussions.

References and Notes

(1) Crespo-Hernandez, C. E.; Cohen, B.; Kohler, B. *Nature* **2005**, *436*, 1141−1144.
(2) Perun, S.; Sobolewski, A. L.; Domcke, W. *J. Phys. Chem. A* **2006**, *110*, 9031−9038.
(3) Kim, N. J.; Jeong, G.; Kim, Y. S.; Sung, J.; Kim, S. K.; Park, Y. D. *J. Chem. Phys.*, **2000**, *113*, 10051−10055.
(4) Nir, E.; Kleinermanns, K.; de Vries, M. *Nature* **2000**, *408*, 949−951.
(5) Lührs, D. C.; Viallon, J.; Fischer, I. *Phys. Chem. Chem. Phys.* **2001**, *3*, 1827−1831.
(6) Kang, H.; Jung, B.; Kim, S. K. *J. Chem. Phys.* **2003**, *118*, 6717−6719.
(7) He, Y. G.; Wu, C. Y.; Kong, W. *J. Phys. Chem. A* **2004**, *108*, 943−949.
(8) Ullrich, S.; Schultz, T.; Zgierski, M. Z.; Stolow, A. *J. Am. Chem. Soc.* **2004**, *126*, 2262−2263.
(9) Ullrich, S.; Schultz, T.; Zgierski, M. Z.; Stolow, A. *Phys. Chem. Chem. Phys.* **2004**, *6*, 2796−2801.
(10) Canuel, C.; Mons, M.; Piuzzi, F.; Tardivel, B.; Dimicoli, I.; Elhanine, M. *J. Chem. Phys.* **2005**, *122*, 074316.
(11) Satzger, H.; Townsend, D.; Patchkovskii, S.; Zgierski, M. Z.; Ullrich, S.; Stolow, A. *Proc. Natl. Acad. Sci. U.S.A.* **2006**, *103*, 10196−10201.
(12) Crespo-Hernandez, C. E.; Cohen, B.; Hare, P. M.; Kohler, B. *Chem. Rev.* **2004**, *104*, 1977−2019.
(13) Plützer, C.; Hunig, I.; Kleinermanns, K.; Nir, E.; de Vries, M. S. *Chem. Phys. Chem.* **2003**, *4*, 838−842.
(14) Schultz, T.; Samoylova, E.; Radloff, W.; Hertel, I. V.; Sobolewski, A. L.; Domcke, W. *Science* **2004**, *306*, 1765−1768.
(15) Samoylova, E.; Lippert, H.; Ullrich, S.; Hertel, I. V.; Radloff, W.; Schultz, T. *J. Am. Chem. Soc.* **2005**, *127*, 1782−1786.
(16) Ritze, H. H.; Lippert, H.; Samoylova, E.; Smith, V. R.; Hertel, I. V.; Radloff, W.; Schultz, T. *J. Chem. Phys.* **2005**, *122*, 224320.
(17) Abo-Riziq, A.; Grace, L.; Nir, E.; Kabelac, M.; Hobza, P.; de Vries, M. S. *Proc. Natl. Acad. Sci. U.S.A.* **2005**, *102*, 20−23.
(18) Canuel, C.; Elhanine, M.; Mons, M.; Piuzzi, F.; Tardivel, B.; Dimicoli, I. *Phys. Chem. Chem. Phys.* **2006**, *69*, 3615−3618.
(19) Stert, V.; Radloff, W.; Freudenberg, T.; Noack, F.; Hertel, I.; Jouvet, C.; Dedonder-Lardeux, C.; Solgadi, D. *Europhys. Lett.* **1997**, *40*, 515−520.
(20) Stert, V.; Radloff, W.; Schulz, C.; Hertel, I. *Eur. Phys. J. D* **1999**, *5*, 97−106.
(21) Broo, A. *J. Phys. Chem. A* **1998**, *102*, 526−531.
(22) Nir, E.; Plützer, C.; Kleinermanns, K.; de Vries, M. *Eur. Phys. J. D* **2002**, *20*, 317−329.
(23) Lee, Y.; Schmitt, M.; Kleinermanns, K.; Kim, B. *J. Phys. Chem. A* **2006**, *110*, 11819−11823.
(24) Marian, C. M. *J. Chem. Phys.* **2005**, *122*, 104314.
(25) Perun, S.; Sobolewski, A. L.; Domcke, W. *J. Am. Chem. Soc.* **2005**, *127*, 6257−6265.
(26) Blancafort, L. *J. Am. Chem. Soc.* **2006**, *128*, 210−219.

(27) Zierhut, M.; Roth, W.; Fischer, I. *Phys. Chem. Chem. Phys.* **2004**, *6*, 5178−5183.
(28) Hünig, I.; Plützer, C.; Seefeld, K. A.; Löwenich, D.; Nispel, M.; Kleinermanns, K. *Chem. Phys. Chem.* **2004**, *5*, 1427−1431.
(29) Perun, S.; Sobolewski, A. L.; Domcke, W. *Chem. Phys.* **2005**, *313*, 107−1.
(30) Pancur, T.; Schwalb, N. K.; Renth, F.; Temps, F. *Chem. Phys.* **2005**, *313*, 199−212.
(31) Matsika, S. *J. Phys. Chem. A*, **2004**, *108*, 7584−7590.
(32) Perun, S.; Sobolewski, A. L.; Domcke, W. *J. Phys. Chem. A* **2006**, *110*, 13238−13244.
(33) Kang, H.; Lee, K. T.; Jung, B.; Ko, Y. J.; Kim, S. K. *J. Am. Chem. Soc.* **2002**, *124*, 12958−12959.
(34) Zgierski, M.; Patchkovskii, S.; Fujiwara, T.; Lim, E. *J. Phys. Chem. A* **2005**, *109*, 9384−9387.
(35) Hudock, H.; Levine, B.; Thompson, A.; Satzger, H.; Townsend, D.; Gador, N.; Ullrich, S.; Stolow, A.; Martinez, T. *J. Phys. Chem. A* **2007**, *111*, 8500−8508.
(36) Kabelac, M.; Hobza, P. *J. Phys. Chem. B* **2001**, *105*, 5804−5817.
(37) Plützer, C.; Hünig, I.; Kleinermanns, K.; Nir, E.; de Vries, M. *Chem. Phys. Chem.* **2003**, *4*, 838−842.
(38) Sobolewski, A. L.; Domcke, W.; Hattig, C. *Proc. Natl. Acad. Sci. U.S.A.* **2005**, *102*, 17903−17906.
(39) Samoylova, E.; Smith, V. R.; Ritze, H. H.; Radloff, W.; Kabelac, M.; Schultz, T. *J. Am. Chem. Soc.* **2006**, *128*, 15652−15656.
(40) Blanchet, V.; Zgierski, M.; Seideman, T.; Stolow, A. *Nature* **1999**, *401*, 52−54.
(41) Stolow, A. *Annu. Rev. Phys. Chem.* **2003**, *54*, 89−119.
(42) Stolow, A.; Bragg, A.; Neumark, D. *Chem. Rev.* **2004**, *104*, 1719−1757.
(43) Hertel, I. V.; Radloff, W. *Rep. Prog. Phys.* **2006**, *69*, 1897−2003.
(44) Samoylova, E.; Smith, V. R.; Ritze, H. H.; Radloff, W.; Hertel, I.; Schultz, T. *Femtochemistry VII, Fundamental Ultrafast Processes in Chemistry, Physics, and Biology*; Elsevier: Amsterdam, 2006.
(45) Bonacic-Koutecky, V.; Brauer, B.; Eberhardt, W.; Gerber, R.; Gonzalez, L.; von Helden, G.; Kammrath, A.; Kim, S.; Manz, J.; Meijer, G.; Mitric, R.; Neeb, M.; Neumark, D.; Schultz, T.; Stanzel, J. *Analysis and Control of Ultrafast Photoinduced Reactions*, volume 87 of *Springer Series in Chemical Physics*; Springer: Heidelberg, 2007.
(46) Hwang, C. T.; Stumpf, C. l.; Yu, Y.-Q.; Kenttämaa, H. I. *Int. J. Mass Spectrom.*, **1999**, *182*/*183*, 253−259.
(47) Hunter, E.; Lias, S. *NIST Chemistry WebBook*; National Institute of Standards and Technology: Gaithersburg, MD, 2005. http://webbook.nist.gov.
(48) Russo, N.; Toscano, M.; Grand, A.; Jolibois, F. *J. Comput. Chem.* **1989**, *19*, 989.
(49) Peng, S.; Padva, A.; LeBreton, P. R. *Proc. Natl. Acad. Sci. U.S.A.* **1976**, *73*, 2966−2968.
(50) Urano, S.; Yang, X.; LeBreton, P. *J. Mol. Struct.* **1989**, *214*, 315−328.
(51) Brady, B.; Peteanu, L.; Levy, D. *Chem. Phys. Lett.* **1988**, *147*, 538.
(52) Kim, S.; Lee, W.; Herschbach, D. *J. Phys. Chem.* **1996**, *100*, 7933−7937.
(53) Lappi, S.; Collier, W.; Franzen, S. *J. Phys. Chem. A* **2002**, *106*, 11446−11455.
(54) Roca-Sanjuán, D.; Rubio, M.; Merchán, M.; Serrano-Andrés, L. *J. Chem. Phys.* **2006**, *125*, 084302.
(55) Nolting, D.; Weinkauf, R.; Hertel, I.; Schultz, T. *Chem. Phys. Chem.* **2007**, *8*, 751−755.